Vortex Filament Model of the Wake Behind a Missile at High Angle of Attack

Andrew H. Van Tuyl*
Naval Surface Weapons Center, Silver Spring, Maryland

A method for calculation of the flow past a missile at high angle of attack is described in which the vortex wake is approximated by means of three-dimensional vortex filaments attached to given open separation lines. The condition of tangential flow on the body is satisfied by use of quadrilateral source panels. Each filament consists of straight-line segments, ending in a semi-infinite segment parallel to the freestream, and is made part of a system of vortices of horseshoe type by means of connecting segments inside the body. The method involves the simultaneous calculation of the rollup and circulations of the vortex filaments, using conditions that hold along the juncture of a separating vortex sheet and the body. Calculations are presented for a blunted ogive cylinder at 10-deg incidence and for a hemisphere cylinder at 19-deg incidence, starting from separation lines obtained by use of the thin-layer Navier-Stokes equations.

Introduction

THE flow past a missile at high angle of attack is difficult to calculate because of the occurrence of three-dimensional flow separation on the leeward portion of the body. Past work, however, has shown that many features of this vortex wake can be calculated by means of potential theory when the separation line is known approximately. Most of these earlier computational methods are based on the impulsive crossflow analogy (Refs. 1–9, for example). Three-dimensional vortex filaments have been used to model the vortex wake behind a wing at high angle of attack (Refs. 10 and 11, e.g.), where separation occurs at subsonic leading edges in addition to the trailing edge. Boundary conditions on the wing in these references were satisfied by use of a vortex lattice. This method has been recently applied to the case of a smooth body with a given separation line,[12–14] where the boundary condition of tangential flow on the body is satisfied either by use of vortex lattice[12,14] or by a combination of a vortex lattice and a source distribution along the axis of the missile.[13] Calculations involving vortex filaments have also been carried out in which the missile boundary condition is satisfied by use of a surface source distribution.[15] In Ref. 15, the strengths and locations of vortex filaments are determined from experiment, and the forces on the body are calculated. Portnoy[16] has suggested an application of vortex filament models to the interactive boundary-layer calculation of separated flow, in which a combination of vortex sheets and vortex filaments is used.

In the present paper, a method for calculation of the vortex wake is given in which it is assumed that the vortex wake can be approximated by vortex sheets attached to the body along given separation lines. Each vortex sheet is replaced by a given number of segmented vortex filaments attached to the body along a given separation line with the flow tangency condition on the body satisfied by use of a surface source distribution. The circulations of the filaments are determined by use of conditions that hold along the juncture of a vortex sheet and a smooth body when vorticity is being shed. These conditions are given by Smith.[17] They lead to an expression for the rate of change of circulation along the separation line with respect to distance which becomes identical with a result given in Ref. 17 when slender-body assumptions are made. The present method differs from those that use a vortex lattice (Refs. 12–14), mainly in the use of the conditions of Ref. 17 for calculation of the circulations of the filaments. Because of the use of a surface source distribution, it is applicable to nonslender bodies. The present method is intended only for the approximate calculation of the vortex wake when separation lines are given and is not concerned with the determination of the separation lines themselves.

Calculations by the present method are presented for a blunted ogive cylinder at 10-deg incidence and for a hemisphere cylinder at 19-deg incidence, starting from separation lines given by the thin-layer Navier-Stokes calculations of Refs. 18 and 19. The surface pressure distributions obtained are compared with those of Refs. 18 and 19 and with experimental data of Ref. 20. These examples are also included in Ref. 21 as part of a comparative study.

Conditions Along a Separating Vortex Sheet

We will consider a missile-type body in a steady incompressible potential flow such that there is a separating vortex sheet on each side of the body attached to a separation line of open type. We will assume that the separation lines are smooth and that the body has a continuously varying tangent plane. Because of the restriction to open separation, the condition of continuity of pressure across a vortex sheet implies continuity of the velocity magnitude. As shown in Fig. 1, when a separating vortex sheet satisfies these conditions, and when in addition vorticity is being shed from the body into the vortex sheet, the following three properties hold:

1) The vortex sheet is tangent to the body.

2) The separation line is a streamline on the downstream side of the vortex sheet, while the velocity at the separation line on the upstream side of the vortex sheet is equal to the upstream velocity on the body.

3) The vortex line at a point of the vortex sheet bisects the angle between the streamlines on opposite sides of the vortex sheet.

The first two properties were shown in Ref. 17, and the third follows from the continuity of the velocity magnitude across the vortex sheet and from symmetry considerations.

As shown in Fig. 2, we will use coordinates ξ, η, and ζ with origin at an arbitrary point of one of the separation lines. Coordinates ξ and η lie in the tangent plane of the body at the origin, with the ξ axis tangent to the separation line as shown. We will first consider the left side of the body when facing the oncoming flow, as shown in Fig. 2a. The corre-

Received June 20, 1986; revision received Sept. 10, 1987.

*Mathematician. Member AIAA.

sponding results for the right side are then obtained by inspection.

Let superscripts 1 and 2 refer to the upstream and downstream sides of the vortex sheet, respectively, and let the upstream velocity at the origin in Fig. 2a be denoted by

$$\boldsymbol{U}^{(1)} = (v_1, v_2, 0) \tag{1}$$

Then from conditions 1 and 2 and the continuity of the velocity magnitude across the vortex sheet, it follows that the downstream velocity at the origin is given by

$$\boldsymbol{U}^{(2)} = (V, 0, 0) \tag{2}$$

where $V = (v_1^2 + v_2^2)^{1/2}$. Let ϕ be the potential of the flow, defined so that the velocity is the gradient of ϕ, and let s be the arc length along the separation line measured from the upstream end. The circulation of the vortex sheet from the beginning ($s = o$) up to the arc length s is given by

$$\Gamma(s) = \int_0^s [\boldsymbol{U}^{(1)} - \boldsymbol{U}^{(2)}] \cdot d\vec{s} \tag{3}$$

From Eqs. (1–3) we find that

$$\frac{d\Gamma}{ds} = v_1 - V \tag{4}$$

at the origin. By multiplying and dividing the right-hand side of Eq. (4) by $V + v_1$, we can also write the preceding equality in the form

$$\frac{d\Gamma}{ds} = -\frac{v_2^2}{V + v_1} \tag{5}$$

Equation (5) can be shown to be equivalent to Eq. (A-10) of Ref. 17 when slender-body assumptions are made and the angle of incidence is small. Proceeding similarly in Fig. 2b, noting that we then have $\boldsymbol{U}^{(2)} = (-V, 0, 0)$ and that v_1 is negative in Fig. 2b, we find that

$$\frac{d\Gamma}{ds} = \frac{v_2^2}{V - v_1} \tag{6}$$

on the right-hand side of the body.

Description of the Vortex Filament Model

As in Fig. 2, we will consider a body at angle of attack α in a Cartesian coordinate system with a freestream velocity of magnitude V_∞ in the positive x direction. We will assume that separation lines are given as separate curves on the left- and right-hand sides of the body, respectively. In the present method, the boundary condition of tangential velocity on the body is satisfied by use of a source distribution on the body surface. The body is covered by quadrilateral panels and, for a given external potential flow, the method of Hess and Smith, as implemented by Dawson and Dean,[22] is used to calculate a constant source density on each quadrilateral. The boundary condition on the body is satisfied at the null point of each quadrilateral, defined as the point at which the velocity due to the quadrilateral alone is normal to the plane of the quadrilateral. The results obtained are nearly the same when the centroid of the quadrilateral is used rather than the null point. The quadrilaterals are determined as in Fig. 3 so that each of the given separation lines passes through the null points or centroids of quadrilaterals at chosen axial stations. Quadrilaterals are not placed on the base of the cylinder, and modeling of the base flow is not considered.

The vortex sheets attached to the body along the given separation lines are approximated by a given number of segmented vortex filaments, each beginning at the null point or centroid of a quadrilateral and ending in a semi-infinite vortex filament parallel to the freestream. Each filament consists of a given number of straight-line segments which may be of unequal lengths. In the present method, the segments nearest the body should have lengths not less than the maximum dimension of the nearby source quadrilaterals. The purpose of this condition is to prevent the velocity at the midpoint of a segment from being determined mainly by a single quadrilateral. In order to prevent strong interactions between closely neighboring filaments, a small cutoff radius is placed about each segment, within which the velocity due to the segment vanishes. More elaborate treatments of cutoff, such as the variable cutoff procedure of Ref. 13, were not investigated.

These filaments can be made part of a system of horseshoe-type vortices in several ways. In the symmetric case, one procedure is to connect symmetrically placed pairs of vortex filaments by straight-line segments inside the body. A second method, applicable to both the symmetric and asymmetric cases, is to connect each filament to the body axis by a segment perpendicular to the axis and to complete each vortex by means of a portion of the axis within the body and a segmented vortex filament outside the body. The latter is common to all the vortices, and its circulation is zero in the symmetric case. These procedures are shown schematically in Fig. 4.

The present method is an iterative one in which two calculations are carried out alternately. In the first calculation,

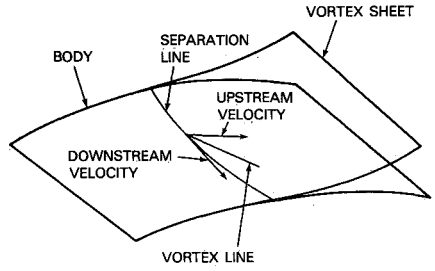

Fig. 1 Streamlines and vortex line on a body at the juncture of a separating vortex sheet.

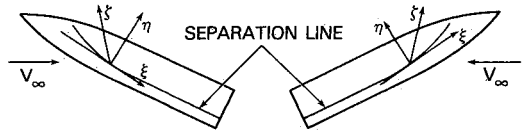

(a) LEFT SIDE OF BODY (b) RIGHT SIDE OF BODY

Fig. 2 Local coordinate systems.

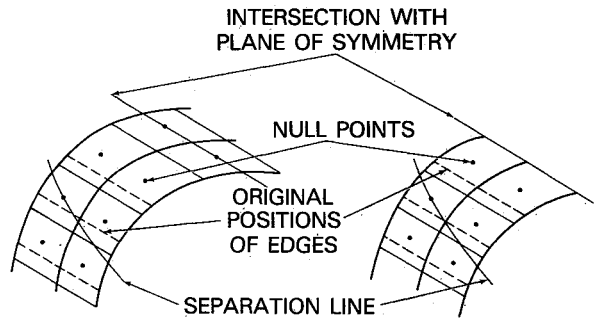

(a) PANELS BISECTED BY PLANE OF SYMMETRY (b) EDGES ON PLANE OF SYMMETRY

Fig. 3 Adjustment of quadrilaterals.

the shapes of the vortex filaments are held constant, and the source densities and the circulations of the filaments are determined simultaneously. In the second calculation, the filaments are made approximately force-free by means of a rollup calculation, with the source strengths and circulations held constant. Initially, the vortex filaments are chosen as semi-infinite straight filaments parallel to the freestream.

Calculation of the Circulations and Source Densities

Let the separation lines in Figs. 2a and 2b be denoted by C_1 and C_2, respectively, with quadrilaterals determined as in Fig. 5 so that N_1 null points lie on C_1 and N_2 on C_2 in the general asymmetric case. Vortex filaments of given shapes are attached to the body at these null points, and vortices of horseshoe type are formed as in Fig. 4. Let s be the arc length along each of the separation lines measured from the upstream end, and let $s = s_i$ at the null points, where $1 \le i \le N_1$ on C_1 and $N_1 + 1 \le i \le N_1 + N_2$ on C_2. In the symmetric case we have $N_1 = N_2$, and it is necessary to consider only the range $1 \le i \le N_1$.

In the present method, the circulation $\Delta\Gamma_i$ of the vortex sheet between the $(i-1)$st and ith null points is concentrated at the ith filament for $2 \le i \le N_1$ and $N_1 + 2 \le i \le N_1 + N_2$. The values of $\Delta\Gamma_1$ and $\Delta\Gamma_{N_1+1}$ are determined by a linear extrapolation procedure to be described later. The circulation along each separation line due to the vortex filaments is seen to be a step function. In particular, the circulation along C_1 is zero for $0 \le s < s_1$ and is equal to $\Delta\Gamma_1 + \Delta\Gamma_2 + \ldots + \Delta\Gamma_{i-1}$ for $s_{i-1} \le s < s_i$, $2 \le i \le N_1$. For given values of $\Delta\Gamma_i$, we can calculate the flow about the body by the procedure used by Dawson and Dean.[22] The flow due to the vortex filaments and the connecting segments is then part of the onset flow on the body and is calculated by use of the Biot-Savart law.

In the present calculation, successive approximations to the circulations and source densities are found by means of an iterative procedure. Let the nth approximation to $\Delta\Gamma_i$ be denoted by $\Delta\Gamma_i^{(n)}$, $n \ge 0$, where the quantities $\Delta\Gamma_i^{(0)}$ are initial guesses. Given the values of $\Delta\Gamma_i^{(n)}$ for a given $n \ge 0$, we obtain new values $\Delta\Gamma_i^{(n+1)}$ as follows. By means of the Hess-Smith procedure, we first calculate the source densities corresponding to the given n and the velocity components $v_{1,i}^{(n)}$ and $v_{2,i}^{(n)}$ at the points of attachment of the filaments. The velocities obtained by linear interpolation at the midpoints of the arcs between successive filaments on each separation line are then given by

$$v_{1,i-1/2}^{(n)} = \left[v_{1,i-1}^{(n)} + v_{1,i}^{(n)} \right]/2$$

$$v_{2,i-1/2}^{(n)} = \left[v_{2,i-1}^{(n)} + v_{2,i}^{(n)} \right]/2 \qquad (7)$$

for $2 \le i \le N_1$ and $N_1 + 2 \le i \le N_1 + N_2$. Substituting Eq. (7) in Eqs. (5) and (6), we obtain

$$\left(\frac{d\Gamma}{ds}\right)_i^{(n)} = -\left[v_{2,i-1/2}^{(n)}\right]^2 \Big/ \left[V_{i-1/2}^{(n)} + v_{1,i-1/2}^{(n)}\right] \qquad (8)$$

along C_1 and

$$\left(\frac{d\Gamma}{ds}\right)_i^{(n)} = \left[v_{2,i-1/2}^{(n)}\right]^2 \Big/ \left[V_{i-1/2}^{(n)} - v_{1,i-1/2}^{(n)}\right] \qquad (9)$$

along C_2, where

$$V_{i-1/2}^{(n)} = \left\{ \left[v_{1,i-1/2}^{(n)}\right]^2 + \left[v_{2,i-1/2}^{(n)}\right]^2 \right\}^{1/2} \qquad (10)$$

Finally, we have

$$\Delta\Gamma_i^{(n+1)} = \left(\frac{d\Gamma}{ds}\right)_i^{(n)} \Delta s_i \qquad (11)$$

for $2 \le i \le N_1$ and $N_1 + 2 \le i \le N_1 + N_2$, where $\Delta s_i = s_i - s_{i-1}$. The quantities $\Delta\Gamma_i^{(n+1)}$ may be calculated in any order. In the symmetric case we have $\Delta\Gamma_i = -\Delta\Gamma_{N_1+i}$, and it is necessary to calculate new values $\Delta\Gamma_i^{(n+1)}$ only for $1 \le i \le N_1$.

We calculate $\Delta\Gamma_1$ from $\Delta\Gamma_2$ and $\Delta\Gamma_{N_1+1}$ from $\Delta\Gamma_{N_1+2}$ by extrapolation, assuming that the circulation of the vortex sheet decreases to zero linearly with respect to s at the upstream end of each separation line. We then have

$$\Delta\Gamma_1 = s_1 \Delta\Gamma_2 / \Delta s_1 \qquad (12)$$

on C_1 and

$$\Delta\Gamma_{N_1+1} = s_{N_1+1} \Delta\Gamma_{N_1+2} / \Delta s_{N_1+1} \qquad (13)$$

on C_2.

At the beginning of the calculation, it is convenient to take the quantities $\Delta\Gamma_i^{(o)}$ to be equal. Examples show that convergence is usually rapid, and that the number of iterations required for convergence is not very sensitive to the initial guess. In particular, convergence is obtained when the $\Delta\Gamma_i^{(o)}$ are zero.

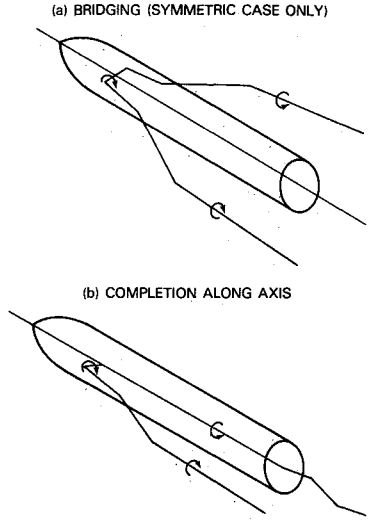

Fig. 4 Formation of vortices from vortex filaments.

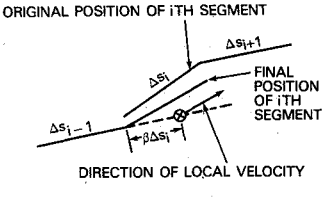

Fig. 5 Procedure for rollup calculation.

The Rollup Calculation

The purpose of the rollup calculation is to determine the positions of the vortex segments so that they are nearly force-free. In Ref. 10 and in Refs. 12–14, this is approximately done by making each segment parallel to the local velocity at the upstream endpoint of the segment. An alternate procedure is described in Ref. 11 in which each segment is made approximately parallel to the local velocity at an intermediate point of the segment. As shown in Fig. 5, the local velocity is calculated at a point on the extension of the previous segment at a distance $\beta\Delta s_i$ from the upstream endpoint, with $0 \le \beta \le 1$. The case $\beta = 0$ corresponds to the first

procedure described. Numerical experiments in Ref. 11 indicate that for vortex segments of a given length, the greatest accuracy is obtained when β is approximately equal to 0.5.

The present method uses the procedure of Ref. 11 with $\beta = 0.5$ at segments not attached to the body, and is described as follows. During a given iteration, the filaments are modified in the order of increasing i. When a given filament is modified, it is changed segment by segment starting at the body. The first segment is made tangent to the body at a null point, such that it is parallel to the direction of the vortex line passing through the null point. As shown in Fig. 1, this vortex line bisects the angle between the upstream velocity at the null point and the separation line. This segment is seen not to be force-free, but calculations show that there is little change in the flow due to small changes in the orientations of the initial segments. The remaining segments are then moved in order by the procedure of Fig. 4 until the modification of the given filament is complete. The final segment is a semi-infinite segment parallel to the freestream direction. The velocity of the segment being moved is not included in the calculation of the local velocity.

The convergence obtained at a given segment during an iteration was measured by the greater of the distances through which the endpoints of the segment moved. The rate of convergence was found to decrease strongly when either the number of filaments or the number of segments on each filament was increased. In particular, rapid convergence was found in the case of five vortex filaments attached to each separation line, while much slower convergence was obtained with 10 filaments on each side. In the latter case, good convergence was found near the body after several iterations, while convergence to only one or two figures was obtained at the segments farthest downstream. The slower convergence at downstream segments is due to the smaller magnitudes of the transverse components of velocity there. The effect of these segments at the body is found to change very little between iterations.

Development of the Computer Programs

The computer programs used in the present calculations are based in part on modifications of the programs PFP1 through PFP5 of Ref. 22. The calculation of quadrilaterals is carried out by means of the program PFP1, modified by changes in input-output statements. The input to PFP1 is calculated as shown in Fig. 3, so that the given separation line passes through the null points of quadrilaterals at selected axial stations.

The matrix of influence coefficients used to obtain the source densities is calculated by the procedure used in the program PFP2 of Ref. 22. Calculation of the source densities is then carried out by use of a modification of the program PFP3. When the iterative procedure for determination of the circulations and source densities has converged sufficiently, the flow is calculated at all null points by means of a modification of the program PFP4 of Ref. 22. The velocity at external points due to the quadrilaterals and vortex filaments is calculated by means of a modification of the program PFP5 of Ref 22. The latter has been reorganized extensively, reducing the computation time by about 20%.

Numerical Results

Results have been obtained on the CDC 170/720 for a 10% spherically blunted ogive cylinder at 10-deg incidence and for a hemisphere cylinder at 19-deg incidence, using separation lines obtained from thin-layer Navier-Stokes calculations.[18,19] The latter were carried out at a freestream Mach number $M_\infty = 0.2$ corresponding to nearly incompressible flow and at a Reynolds number of 10^5. The ogive cylinder had an overall length of 11 calibers and a nose length of three calibers before blunting, and the hemisphere cylinder had a length of five calibers.

Let R be the radius of the cylindrical portion of each body, let x be the distance along the axis measured from the nose, and let θ be the azimuthal angle in degrees measured from the windward portion of the plane of symmetry. Then the equation of the separation line on the blunted ogive cylinder used in the present calculations is given by[18]

$$\theta = 110 + e^{-0.97x_1^{1/2}}\left(1928.792 - 1115.694x_1^{1/2} + 149.925x_1\right) \tag{14}$$

for $x_1 > 6.6$, where $x_1 = x/R$. The coefficients in Eq. (14) were obtained from the results of Ref. 18 by means of a least-squares fit. Similarly, the equation of the separation line on the hemisphere cylinder is given by

$$\theta = 98.6 + e^{-1.5x_1^{1/2}}\left(481.351 - 229.558x_1^{1/2} + 21.250x_1\right) \tag{15}$$

for $x_1 > 2.7$.[19] The maximum deviation of these fits from the separation lines obtained by the thin-layer Navier-Stokes calculations is about 3%.

Both types of quadrilateral configurations shown in Fig. 3 were used in the present calculations. For convenience, the configurations corresponding to Figs. 3a and 3b will be referred to in the following as QD1 and QD2, respectively. The spherical portion of each body was covered by 48 quadrilaterals, with 24 on each side of the plane of symmetry in both QD1 and QD2. The separation lines do not lie on the spherical portions of the body in the present cases; hence, it is not necessary to rotate quadrilaterals there. The configuration QD1 was used for both the blunted ogive cylinder and the hemisphere cylinder, while QD2 was used only in the case of the blunted ogive cylinder. In the configuration QD1, the total number of quadrilaterals on the blunted ogive cylinder was 408 without symmetry and 234 when symmetry is taken into account. The corresponding numbers for the hemisphere cylinder were 312 and 176. In the configuration QD2, the number of quadrilaterals on one side of the plane of symmetry of the blunted ogive cylinder was 204.

The number of filaments on one side of the body in the present calculations was 12 in the case of the blunted ogive cylinder and 9 in the case of the hemisphere cylinder. Each filament consisted of 17 segments of unequal lengths where the segment lengths increased from 1.0 for the first five segments to 2.0 for the last five. The configuration QD2 for the blunted ogive cylinder is shown in Fig. 6.

In each case, the source densities and circulations were first calculated with the filaments parallel to the freestream. Two more calculations of source densities and circulations were then carried out, each preceded by a rollup calculation of seven iterations. Complete convergence of the rollup calculation was not obtained, but convergence to several significant figures occurred near the body. The procedure of Fig. 4a for the formation of horseshoe-type vortices was used in the

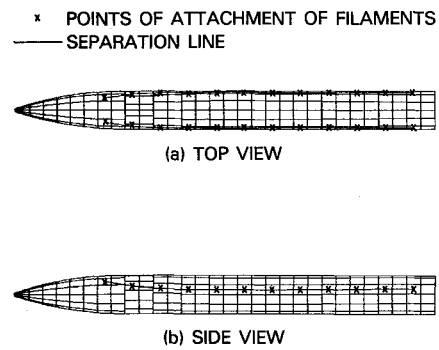

Fig. 6 Quadrilateral configuration QD2 on blunted ogive cylinder.

present calculations. However, some of the calculations were repeated using the procedure of Fig. 4b, and agreement to three or four decimal places was found.

In the calculation of source densities and circulations, convergence to five or six figures was always found after six iterations. Fewer than six iterations were usually sufficient in the second and third calculations because of improved initial guesses. In Tables 1–3, the circulations of the filaments on the right side of the body are given for the three cases calculated. In each table, the circulations are given after each calculation of source densities and circulations. The circulations on the left sides of the bodies are the negatives of those shown. These tables indicate convergence in each case as the number of calculations of source densities and circulations increases, with the slowest convergence at the filaments farthest downstream. This is consistent with the incomplete convergence of the rollup calculation. The leading vortex filaments were slightly upstream of the beginning of separation on each body, as seen from Tables 1–3. The circulations of these filaments are very small, however, and small changes in their positions have negligible effect on the flow at the body.

Figure 7 gives the circumferential pressure distributions on the blunted ogive cylinder at several axial stations obtained by the vortex filament method and the thin-layer Navier-Stokes calculations. Axial distances are denoted by x/D, where $D = 2R$ is the diameter of the cylinder. The pressure is also shown for the potential flow solution, which is found by using the same quadrilateral configurations but with the vortex filaments omitted. At $x/D = 0.9$ and $x/D = 2.0$, the results obtained by the vortex filament method nearly coincide with the potential flow results, and hence, only the former are shown. Close agreement between the vortex filament and thin-layer results is also found at these stations, except near $\theta = 0$ deg and $\theta = 180$ deg at $x/D = 2.0$. At $x/D = 3.8$ and $x/D = 7.5$, the largest discrepancy between the results obtained by the vortex filament method and the thin-layer calculations is found near $\theta = 0$ deg, while the vortex filament results are in good agreement with those obtained by the thin-layer calculations near $\theta = 180$ deg. The potential flow results are nearly equal to the vortex filament results at these stations up to about $\theta = 90$ deg and are larger near $\theta = 180$ deg.

Figure 8 gives the meridional pressure distributions on a blunted ogive cylinder at $\theta = 0$, 90, and 180 deg calculated by the same three methods as in Fig. 7. The vortex filament calculations were carried out using only the configuration QD1. The pressures at $\theta = 90$ deg were obtained by quadratic interpolation, since the centroids that were originally at 90 deg were rotated during calculation of the quadrilateral input data by the procedure of Fig. 3a. When $\theta = 0$ deg, the pressures calculated by the vortex filament method are seen to be nearly the same as the potential flow results and to be lower than the

Table 1 Circulations $\Delta\Gamma_i/V_\infty R$ and axial locations x_i/R of filaments on the right side of a blunted ogive cylinder at 10-deg incidence using quadrilateral configuration QD1

		Number of source density calculations		
i	x_i/R	1	2	3
1	4.72	0.003	0.003	0.003
2	6.15	0.045	0.044	0.044
3	7.63	0.063	0.063	0.063
4	9.10	0.060	0.061	0.061
5	10.58	0.053	0.053	0.053
6	12.05	0.047	0.050	0.050
7	13.52	0.043	0.049	0.050
8	15.00	0.041	0.045	0.048
9	16.47	0.039	0.044	0.047
10	17.95	0.037	0.042	0.043
11	19.42	0.035	0.040	0.043
12	20.89	0.033	0.036	0.039

Table 2 Circulations $\Delta\Gamma_i/V_\infty R$ and axial locations x_i/R of filaments on the right side of a blunted ogive cylinder at 10-deg incidence using quadrilateral configuration QD2

		Number of source density calculations		
i	x_i/R	1	2	3
1	4.72	0.003	0.003	0.003
2	6.15	0.051	0.050	0.050
3	7.63	0.061	0.061	0.061
4	9.10	0.057	0.059	0.059
5	10.58	0.051	0.054	0.054
6	12.05	0.046	0.050	0.050
7	13.52	0.043	0.045	0.045
8	15.00	0.040	0.042	0.042
9	16.47	0.038	0.042	0.041
10	17.95	0.037	0.040	0.040
11	19.42	0.035	0.038	0.039
12	20.89	0.032	0.034	0.035

Table 3 Circulations $\Delta\Gamma_i/V_\infty R$ and axial locations x_i/R of filaments on the right side of a hemisphere cylinder at 19-deg incidence using quadrilateral configuration QD1

		Number of source density calculations		
i	x_i/R	1	2	3
1	2.13	0.024	0.023	0.023
2	3.03	0.128	0.126	0.126
3	3.93	0.128	0.127	0.127
4	4.83	0.114	0.117	0.118
5	5.73	0.105	0.113	0.113
6	6.63	0.099	0.107	0.106
7	7.53	0.094	0.100	0.099
8	8.43	0.088	0.093	0.091
9	9.33	0.080	0.084	0.083

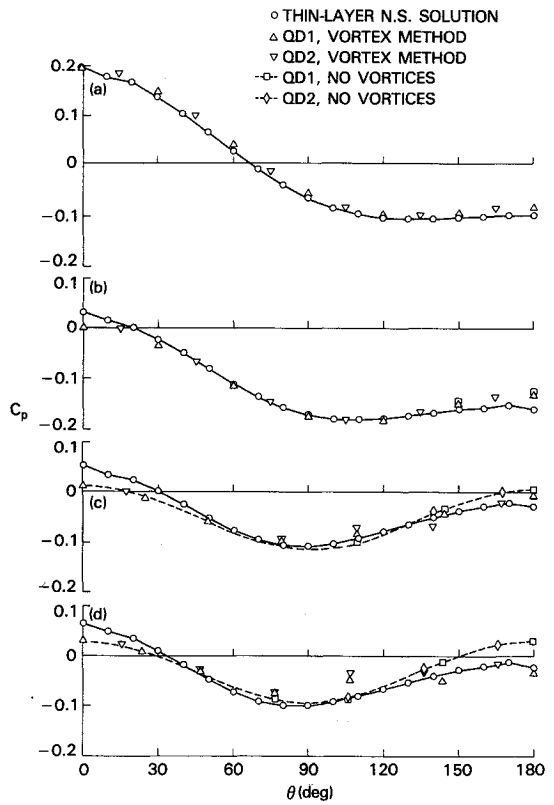

Fig. 7 Circumferential pressure distributions on a 10% blunted ogive cylinder at 10-deg incidence; a) $x/D = 0.9$, b) $x/D = 2.0$, c) $x/D = 3.8$, d) $x/D = 7.5$.

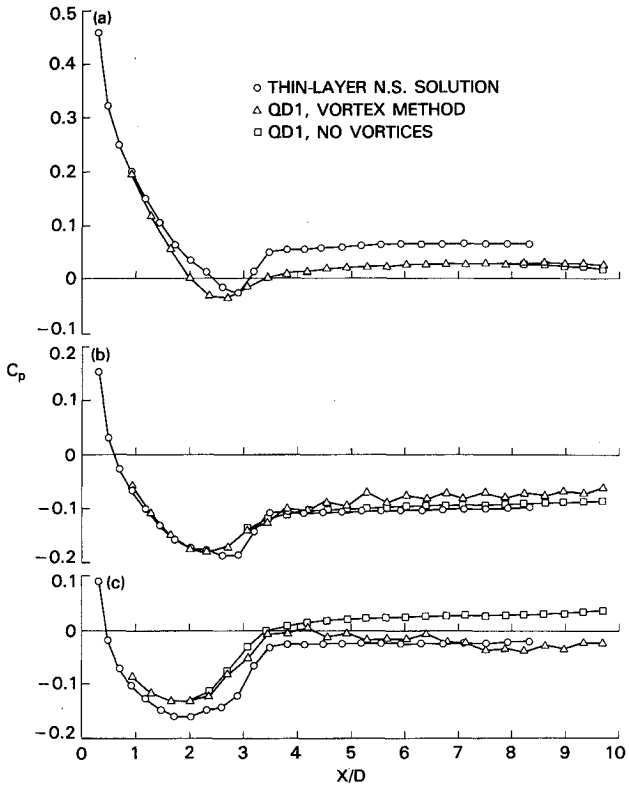

Fig. 8 Meridional pressure distributions on a 10% blunted ogive cylinder at 10-deg incidence; a) θ = 0 deg, b) θ = 90 deg, c) θ = 180 deg.

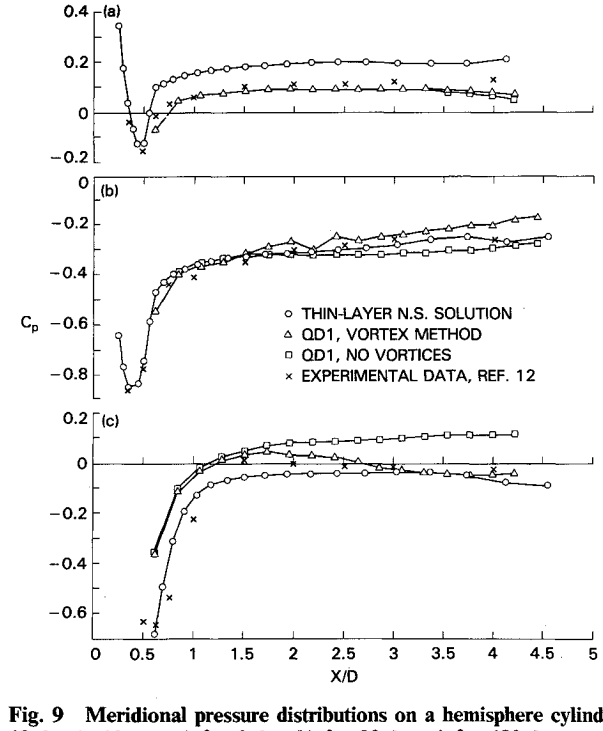

Fig. 9 Meridional pressure distributions on a hemisphere cylinder at 19-deg incidence; a) θ = 0 deg, b) θ = 90 deg, c) θ = 180 deg.

thin-layer values by a nearly constant amount. At $\theta = 90$ deg, the thin-layer and potential flow results nearly coincide throughout. The pressures calculated by the vortex filament method are nearly equal to the other results near the nose and are slightly higher on the back part of the body. At $\theta = 180$ deg, good agreement is found between the vortex filament and thin-layer results on the back part of the body, while the potential flow pressures are much higher.

Finally, the meridional pressure distributions on the hemisphere cylinder obtained by the thin-layer, vortex filament, and potential flow calculations are shown in Fig. 9. As before, only the configuration QD1 was used. The trends in Fig. 9 are seen to be similar to those found for the blunted ogive cylinder in Fig. 8. In addition, experimental data from Ref. 20 at $M_\infty = 0.6$ are included. We see that the data agree best with the vortex filament results when $\theta = 0$ deg and that they agree well with both the vortex filament and thin-layer results when $\theta = 90$ and 180 deg.

Summary and Conclusions

A model of the vortex wake behind a missile at high angle of attack has been described in which it is assumed that the effect of the vortex wake can be approximated by vortex sheets attached to the body along open separation lines. The vortex sheets are replaced by a given number of segmented vortex filaments, and the circulations of the filaments are determined by use of the relations that hold along the juncture of a separating vortex sheet and the body. In the present paper, this model is used for calculation of the flow past the body when open separation lines are given. The calculational procedure has been described in the general asymmetric case, when the separation lines on the two sides of the body are different.

Calculations have been carried out for a slightly blunted ogive cylinder at 10-deg incidence and for a hemisphere cylinder at 19-deg incidence using separation lines obtained from thin-layer Navier-Stokes calculations. In the latter calculations, the separation lines obtained were of open type except for a nose separation bubble near the shoulder of the hemisphere cylinder. Comparison of calculated surface pressure has been made with these calculations and with experimental data for a hemisphere cylinder at 19-deg incidence at $M_\infty = 0.6$. Good agreement with both the thin-layer Navier-Stokes calculations and the experimental data was found on the leeward portions of the bodies toward the back. On the windward sides of the bodies, however, good agreement was found with the experimental data but not with the thin-layer Navier-Stokes calculations. The calculated pressures on the windward sides nearly coincide with the potential flow results. The results on the windward sides of the bodies are therefore not conclusive, but it follows that the present model leads to reasonable results on the leeward sides of the bodies considered.

The separation lines in these examples were obtained by curve fits, starting from the calculations of Refs. 18 and 19. These examples were selected for test purposes because of the availability of surface pressures consistent with the separation lines. The results obtained indicate that the thin-layer approximation was adequate in these cases and that the vortex wakes can be approximated by vortex sheets. In each of these examples, the distribution of panels was rather coarse and the number of filaments was small. A larger computer would allow the use of more panels and larger numbers of filaments and segments.

Acknowledgments

This work was sponsored by the Naval Sea Systems Command under the cognizance of L. Pasiuk. The author wishes to thank A. G. Werschulz for assistance in the modification of the XYZ Potential Flow Program.

References

[1] Hill, J.A.F., "A Nonlinear Theory of the Lift on Slender Bodies of Revolution," *Proceedings of the U.S. Navy Symposium on Aeroballistics*, NAVORD Rep. 5338, Oct. 1954.

[2] Bryson, A.E. Jr., "Symmetric Vortex Separation on Circular Cylinders and Cones," *Journal of Applied Mechanics*, Vol. 26, Dec. 1959, pp. 643–648.

[3]Schindel, L.H., "Effects of Vortex Separation on the Lift Distribution on Bodies of Elliptic Cross Section," *Journal of Aircraft*, Vol. 6, Nov.–Dec. 1969, pp. 537–543.

[4]Angelucci, S.B., "A Multi Vortex Method for Axisymmetric Bodies at Angle of Attack," *Journal of Aircraft*, Vol. 8, Dec. 1971, pp. 959–966.

[5]Angelucci, S.B., "Multi Vortex Model for Bodies of Arbitrary Cross Sectional Shapes," AIAA Paper 73-104, 1973.

[6]Wardlaw, A.B. Jr., "Prediction of Normal Force, Pitching Moment, and Yaw Force on Bodies of Revolution at Angles of Attack up to 50 Degrees Using a Concentrated Vortex Flow-Field Model," NOLTR 73-209, Oct. 1973.

[7]Wardlaw, A.B. Jr., "Multivortex Model of Asymmetric Shedding on Slender Bodies at High Angles of Attack," AIAA Paper 75-123, Jan. 1975.

[8]Deffenbaugh, F.D. and Marshall, F.J., "Time Development of the Flow about an Impulsively Started Cylinder," *AIAA Journal*, Vol. 14, July 1976, pp. 908–913.

[9]Deffenbaugh, F.D. and Koerner, W.G., "Asymmetric Wake Development and Associated Side Forces on Missiles at High Angles of Attack," AIAA Paper 76-364, July 1976.

[10]Mook, D.T. and Maddox, S.A., "Extension of a Vortex-Lattice Method to include the Effects of Leading Edge Separation," *Journal of Aircraft*, Vol. 11, Feb. 1974, pp. 127–128.

[11]Maskew, B., "A Quadrilateral Vortex Method Applied to Configurations with High Circulation," *Vortex-Lattice Utilization*, NASA SP-405, May 1976, pp. 163–186.

[12]Almosnino, D. and Rom, J., "Calculation of Symmetric Vortex Separation Affecting Subsonic Bodies at High Incidence," *AIAA Journal*, Vol. 21, March 1983, pp. 398–406.

[13]Almosnino, D., "High Angle of Attack Calculations of the Subsonic Vortex Flow on Slender Bodies," *AIAA Journal*, Vol. 23, Aug. 1985, pp. 1150–1156.

[14]Thrasher, F.D., "Application of the Vortex-Lattice Concept to Flows with Smooth-Surface Separation," 1982 ONR Symposium on Naval Hydromechanics, Ann Arbor, MI, Aug. 1982.

[15]Sheffield, J.S. and Deffenbaugh, F.D., "A Three Dimensional Vortex Wake Model for Missiles at High Angles of Attack," TRW Report 30584-6003-RU-00, Jan. 1979, or NASA CR 3208, Jan. 1980.

[16]Portnoy, H., "The Position of Laminar Separation Lines on Smooth Inclined Bodies," *AIAA Journal*, Vol 23, June 1985, pp. 956–958.

[17]Smith, J.H.B., "Behaviour of a Vortex Sheet Separating from a Smooth Surface," R.A.E. TR 77058, April 1977.

[18]Chien, K.-Y. and Hsieh, T., "Navier-Stokes Calculation for a Body of Revolution at Incidence," presented at the Second Symposium on Numerical and Physical Aspects of Aerodynamic Flows, Jan. 17–20, 1983.

[19]Chien, K.-Y., private communication, Dec. 1982.

[20]Hsieh, T., "An Investigation of Separated Flow about a Hemisphere-Cylinder at 0 to 19 Degree Incidence in the Mach Number Range from 0.6 to 1.5," AEDC-TR-76-112, Nov. 1976.

[21]Chien, K.-Y., Van Tuyl, A.H., and Hsieh, T., "Prediction of Flowfields About Bodies of Revolution at Large Incidence," *Journal of Spacecraft and Rockets*, Vol. 23, May–June 1986, pp. 245–250.

[22]Dawson, C.W. and Dean, J.S., "The XYZ Potential Flow Program," Naval Ship Research and Development Rept. 3892, June 1972.